Journal of Biomechanics 46 (2013) 1938–1942

Contents lists available at SciVerse ScienceDirect

Journal of Biomechanics

journal homepage: www.elsevier.com/locate/jbiomech
www.JBiomech.com

Short communication

Method for non-optical quantification of in situ local soft tissue biomechanics

Grant M. Tarsi [a,b,1], Russell A. Gould [a,1], Jaebum A. Chung [c], Andrew Z. Xu [c], Alper Bozkurt [b], Jonathan T. Butcher [a,*]

[a] Department of Biomedical Engineering, Cornell University, Ithaca, NY 14853, USA
[b] Department of Electrical and Computer Engineering, North Carolina State University, Raleigh, NC 27695, USA
[c] Department of Applied Engineering Physics, Cornell University, Ithaca, NY 14853, USA

ARTICLE INFO

Article history:
Accepted 20 May 2013

Keywords:
Flexible electronics
Microelectrode device
Pipette aspiration
Biopsy
Diagnosis

ABSTRACT

Soft tissues exhibit significant biomechanical changes as they grow, adapt, and remodel under a variety of normal and pathogenic stimuli. Biomechanical measurement of intact soft tissues is challenging because of its large strain and nonlinear behavior. Tissue distention through applied vacuum pressure is an attractive method for acquiring local biomechanical information minimally invasive and non-destructive, but the current requirement for optical strain measurement limits its use. In this study, we implemented a novel flexible micro-electrode array placed within a cylindrical probe tip. We hypothesized that upon tissue distention, contact with each electrode would result in a precipitous voltage drop (from the resistive connection formed between input and output electrodes) across the array. Hence, tissue distention (strain) can be derived directly from the electrode array geometry. In pilot studies, we compared the electrode array measurements directly against optical deformation measurements in-situ of agar tissue phantoms and freshly isolated porcine tissue. Our results demonstrate that the probe derived stress–strain profiles and modulus measurements were statistically indistinguishable from optical measurement. We further show that electrode geometry can be scaled down to 50 μm in size (length and width) and spaced 50 μm apart without impairing measurement accuracy. These results establish a promising new method for minimally invasive local soft tissue biomechanical measurement, which may be useful for applications such as disease diagnosis and health monitoring.

1. Introduction

Tissue rigidity (often characterized as stiffness or effective modulus) changes significantly during growth, maturation, disease pathogenesis, and healing (Fung, 1993). Biomechanical analyses in clinical settings have been performed for centuries through the use of palpation, which qualitatively assesses tissue resistance to tactile loading (Laughon et al., 2011; Kolb et al., 2002). For deeper tissues, clinicians rely on non-invasive imaging modalities (ultrasound, CT, MRI) to visualize tissues and infer pathological characteristics, if possible. However, these strategies are limited to quantifying linear material responses that are not present in most soft tissues (Robben et al., 2005; Ichikawa et al., 2010). Alternative approaches using finite element analysis of imaging datasets require material model assumptions for all regions of interest, resulting in significant time and resource costs (Celi et al., 2011; Kauer et al., 2002; Samani and Plewes, 2007).

Few devices exist to measure biomechanics of intact soft tissues, the most common being surface indentation (Dawes-Higgs et al., 2004; Brommer et al., 2006). Alternatively, negative pressure can be applied locally through a hollow member, creating a uniaxial tensile test on the distended tissue (Jemec et al., 2001; Buskohl et al., 2012). The principle challenge is measuring the tissue deformation. Transparent shafts permit optical measurement of strain (Butcher et al., 2007), but this limits investigation to accessible tissue surfaces. For example, Nava et al. (2004) implemented a mirror to reflect tissue distention to a video camera, but also increased the device size and thereby its invasiveness. Electrical changes can also characterize soft tissue distention. Microscale strain gauges have been implemented in soft and hard tissues to convert deflections into resistance changes (Jensen et al., 2012). Additionally, microfabricated electrode sensors have been used to monitor electrical currents deep within tissues such as cardiac muscle (Shen et al., 2010).

We here tested the hypothesis that soft tissue distention under local negative pressure could be measured by resistance changes

* Corresponding author. Tel.: +1 607 255 3575.
E-mail address: jtb47@cornell.edu (J.T. Butcher).
[1] Authors with equal contribution.

0021-9290/$ - see front matter © 2013 Elsevier Ltd. All rights reserved.
http://dx.doi.org/10.1016/j.jbiomech.2013.05.014

in electrodes at discrete intervals. In this study, we developed and evaluated a novel small-bore probe with an internal microelectrode array to quantify local soft.

2. Materials and methods

2.1. Probe design

Paired arrays containing six gold-plated electrodes (square with 50–200 μm side lengths) and inter-electrode spacing from 50 to 200 μm were fabricated on printable flexible circuit board (Cornell MEMS Group) (Fig. 1A,B). Arrays were mounted parallel to each other inside the tip of cylindrical borosilicate glass tubing (4 or 10 mm in diameter). Each electrode pair communicated independently via a 6-pin micro-FFC connector that interfaced with a data acquisition system (USB2250, Validyne Inc.). A syringe pump generated negative vacuum pressure (Alladin-2000, WPI Inc.) through the probe cylinder via silicone tubing (Fig. 1C). Negative pressure was monitored via a diaphragm transducer (Validyne, Inc.).

2.2. Quantification of tissue distention

Electrode channels were integrated into a 5 V voltage divider circuit (Fig. 1D). Voltage changes were continuously recorded for each electrode pair while negative pressure was applied to distend the tissue (Figs. 1E and 2A). Output voltage dropped when tissue contacted each electrode pair, due to the resistive connection formed between input and output electrodes (Fig. 2B). These precipitous drops in voltage precisely determined the first contact with a given pair, and output voltage changed little as tissue distended further across each pair (Fig. 2C). Tissue strain was thereby determined at the leading edge of each electrode pair by referencing the electrode's fabricated distance from the device tip. These strains were co-registered with continuous pressure measurements to determine stress–strain data curves as previously described (Buskohl et al., 2012).

2.3. Agarose phantom tests

Agarose gels between 0.75 and 1.5% w/v were tested initially as tissue phantoms with homogenous biomechanical properties. The probe tip was positioned perpendicular to the hydrogel surface with a micromanipulator (World Precision Instruments, Inc.) (Figs. 1E and 2A). Optical imaging was performed simultaneously via stereo-dissection microscope (Discovery-V20, Zeiss, Inc.; Image Pro Software, Spectra Services, Inc.). Voltage, pressure, and digital images were recorded continuously until all electrode pairs were contacted. Resulting pressure and deformation data from each trial were fit to a Fung-based 1st Piola Stress model,

$$P'' = \alpha C E'' e^{(\alpha E''^2)}$$

with Green's strain E'' defined as:

$$E'' = \frac{1}{2}(\lambda^2 - 1)$$

and material coefficients α and C, where $\alpha \times C$ defines an effective modulus of the tissue as previously described (Butcher et al., 2007).

2.4. In situ tissue tests

Direct mechanical tests were conducted on intact lung, liver, and myocardium tissue specimens obtained from freshly slaughtered pigs (~200 kg, Shirk Meats, Inc.). Samples were flushed with ice cold PBS, stored in sterile PBS at 4 °C and tested within 24 h. Tissue segments were cut to fit inside a 100 mm petri dish without disturbing the surface. The free wall of the left ventricle was chosen for heart tissue, while segments from midsections of intact lobes were used for liver and lung. Tissue was kept hydrated but not submerged with PBS. All tissues were preconditioned with 10 cycles of loading to approximately 10% of deformation, followed by quasi-static loading up to 60 kPa.

2.5. Statistics

Stress–strain data generated from the probe was compared against optical strain based measurement. Data from at least six independent experiments were tested for each probe configuration. Material response curve fits were fit using nonlinear regression as previously described (Butcher et al., 2007). Effective moduli were compared using Analysis of Variance (ANOVA) followed by Tukey post-hoc tests and error bars reported as standard error. $P < 0.05$ determined statistical significance.

3. Results

3.1. Probe design analysis

Tissue was distended into the probe through a negative vacuum pressure, and a precipitous drop in voltage was recorded for every electrode pad in sequential order corresponding with increased vacuum pressure (Fig. 2A and B). We determined that an electrode size of 50 μm in length, width, and spacing ($50 \times 50\_50$) was capable of recording tissue contact. Tests using arrays with different inter-electrode spacing ($50 \times 50\_50$ vs. $100 \times 100\_100$)

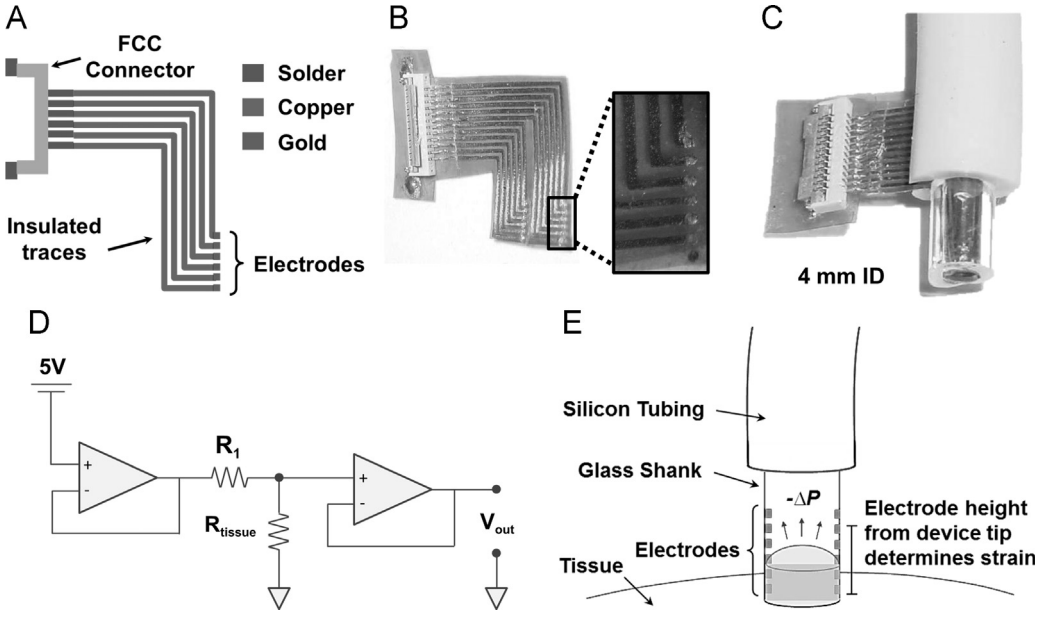

Fig. 1. Aspiration probe design. (A) Gold coated microelectrodes were connected to insulated traces and soldered to an FCC connector. (B) Each electrode was arranged vertically on a flexible PCB such that they extended along the axial length of the glass shank, with the bottom of the PCB flush with the outer edge of the device tip (C). Each probe contained two arrays directly opposite one another. Electrodes at matching heights were paired and inserted into a voltage divider circuit (D) that changed output voltage upon tissue incidence. E) Schematic of probe and tissue loading during aspiration testing.

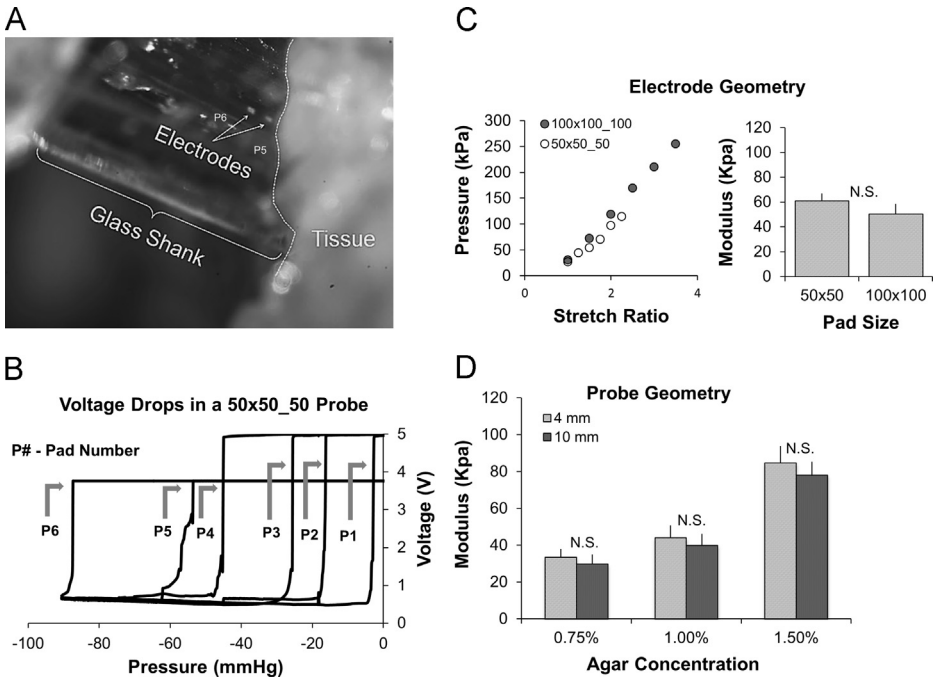

Fig. 2. Demonstration of electrical measurement of tissue deformation. (A) Negative pressure forced tissue distension within the probe and contacted the electrode pairs. (B) Pad specific voltage tracings using a 50×50 μm sized pad array spaced 50 μm apart ($50 \times 50\_50$). Channel output voltage is constant at 5 V until tissue contact is established, after which it drops precipitously. (C) Comparison of pressure vs. stretch ratio measurements with different electrode array geometries. (D) Effective modulus of agarose tissue phantoms measured by a 4 or 10 mm diameter probe.

resulted in a similar pressure vs. stretch ratio curves and overlapped at several pad locations (Fig. 2C). The resulting modulus (60.80 ± 6.12 kPa, 50.159 ± 8.49 kPa, respectively) was non-significant indicating that pad size did not affect the biomechanical response. We next determined the pressure vs. stretch ratio curves for different diameter probes (4 and 10 mm) on agarose tissue phantoms (Fig. 2D). For 4 mm probes, we determined the modulus at 0.75% agar (33.45 ± 4.37 kPa), followed by 1.0% agar (44.14 ± 6.61 kPa), and 1.5% agar (84.58 ± 9.09 kPa). These values were statistically insignificant from identical measurements made with 10 mm diameter probes (29.82 ± 5.13 kPa for 0.7%, 39.99 ± 6.13 kPa for 1.0%, and 78.13 ± 4.45 kPa for 1.5%, $P > 0.2$ for each paired comparison). These results support that electrode array based measurement of tissue strain under negative pressure is insensitive to probe diameter, as predicted by our previous studies (Buskohl et al., 2012; Butcher et al., 2007).

3.2. Comparison of in situ soft tissue biomechanics measurement

Independent biomechanical datasets on freshly isolated porcine tissue was obtained simultaneously via optical (Fig. 3A) and probe measurement of strain (Fig. 3B), for direct comparison. Aggregate data from at least 6 samples (Fig. 3A and B, dots) were fit to Fung-type strain energy constitutive models (Fig. 3A and B, solid lines). Optical and probe derived deformation measurement trends compared well for the different tissue types. During biomechanical testing via optical, the effective modulus of porcine heart tissue was most stiff (58.91 ± 3.83 kPa), followed by liver (39.12 ± 3.21 kPa) and lung (5.18 ± 0.7 kPa, $P < 0.05$ for each). Similarly via probe, the effective modulus of porcine heart tissue was most stiff (61.1 ± 7.06 kPa), followed by liver (37.13 ± 2.13 kPa) and lung (6.00 ± 0.94 kPa, $P < 0.05$ for each). However no statistical differences in modulus measurement were found between either measurement approaches for any of these tissues (Fig. 3C). Together, these results indicate that the probe and traditional optical strain measurement will return identical tissue biomechanics data across (at least) this range of tissue modulus.

4. Discussion

Soft issue rigidity is a product of many biological phenomena, including porosity (permeability), amount, orientation and maturity of extracellular matrix fibers, degree of cellularity, cell contractility, and water content (Karsdal et al., 2013). Each of these components initiates locally and changes over development and with disease progression. It has been suggested that local in-situ tissue stiffness measurement may be useful for disease diagnosis and treatment monitoring. This requires direct measurement of local tissue strain under a defined force in real-time. In vivo imaging, can quantify local tissue strain, but inferring tissue stiffness is challenging with heterogeneous tissues that exhibit nonlinear mechanics (Oberai et al., 2009). Clinical screening of in vivo tissue biomechanics is achieved largely through palpation, whereby the region of interest is compressed and resistance to that deformation assessed qualitatively. A non-biased, quantitative approach such as the one presented here is an attractive alternative. Other instruments have been developed to assess compressive tissue mechanics in vivo through local indentation (Hansma et al., 2009; Vasara et al., 2005).

We here present a method of electrical based strain measurement that achieves high-resolution without signal interference or variation with probe diameter. While attractive for hard tissue surface damage such as cartilage, assessment of deeper and/or softer tissue is challenging because the tissue is likely to translate through its connecting fascia in addition to deforming. Local vacuum pressure alleviates this concern by providing means to both secure and test the tissue. Our results indicate that even low stretch ratios ($\lambda < 1.2$) can generate biomechanical distinction between tissues; particularly as soft tissue responses are often nonlinear. Specifically, the probe derived stress-strain profiles and effective modulus measurements were statistically indistinguishable from optical measurement, and resulting stress–strain curves were identical. We further show that electrode geometry can be scaled down to micron size pads and spacing without jeopardizing measurement accuracy.

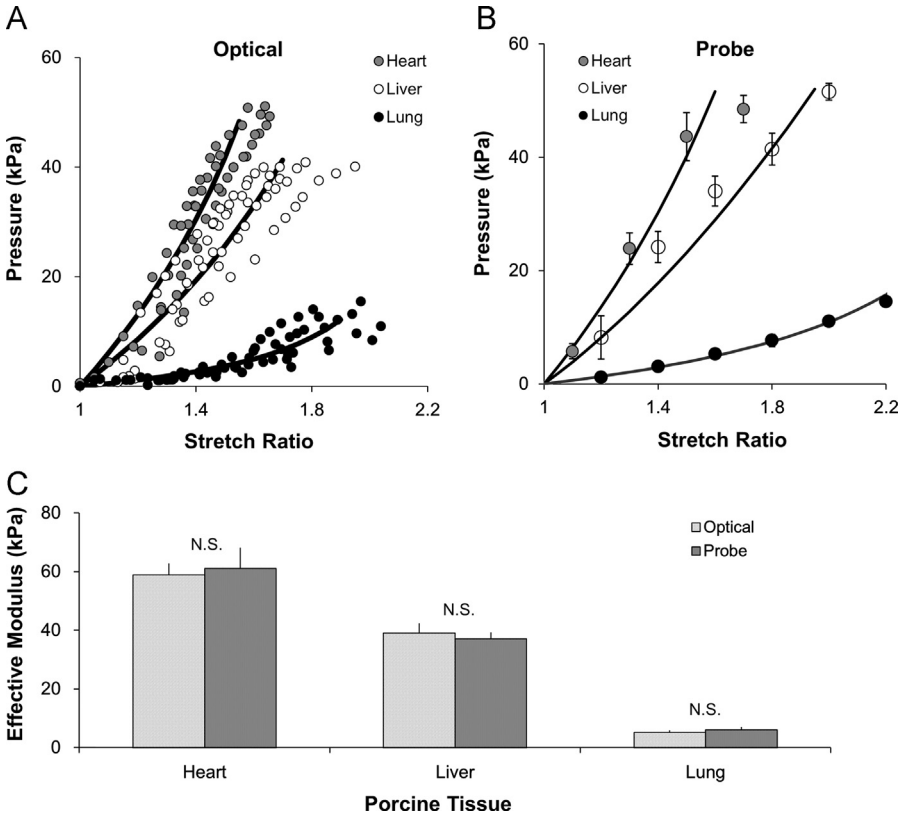

Fig. 3. Direct comparison of optical and electrical based measurement of porcine heart, liver, and lung using vacuum pressure distention. (A) Representative tissue biomechanical measurement (dots) and model fits (solid lines) using optically measured strain. (B) Tissue biomechanics obtained from electrode array based strain measurements. (C) Tissue modulus using the optical vs. probe approaches was statistically insignificant.

Previous computational analyses have determined that this test mimics a uniaxial tensile test of a region two diameters wide and two diameters deep (Michaelson et al., 2002). This test determines an average response across this volume, but if different layers of tissues and/or inclusions/voids exist they will contribute to the resulting biomechanical measurements (Cowin et al., 2002). This possibility for local heterogeneous features should be accounted for when determining the best probe geometry to apply, and balanced against the number of tests needed (which will be more for a smaller probe tip). The diameter of the probe is limited only by the curvature that can be sustained by the flexible electrode array, which for the current designs is about 1 mm. Recent advances with graphene flexible arrays suggest diameters well under 0.1 mm are possible (Yan et al., 2012).

Conversely, measurement of local bulk tissue mechanics may also important if tissue inclusions are often not at the surface (Cowin et al., 2002; Hendricks et al., 2006). Detection of these deeper features is possible with this approach, and may therefore be an attractive complementary diagnostic tool (Kolb et al., 2002). Taken together, the optimal size of the interrogation area will be a function of tissue accessibility, tissue size, and clinical practicality. This non-destructive method is also particularly attractive for sensitive tissues for which removal poses risks to the patient, like lymph nodes, glandular tissue, and densely innervated tissues (Goyal et al., 2008). Alternatively, the probe need not have a long shaft and could be delivered locally through a catheter to test internal lesions such as atherosclerotic plaques or colon polyps. Finally, impedance scanning through the microelectrodes could provide an additional independent parameter for soft tissue assessment (Chauveau et al., 1999).

In conclusion, we present a novel device and method for quantification of soft tissue biomechanics in situ. By tuning the probe geometry and array parameters, a broad range of tissue sizes and locations can be tested. We believe it may be useful independently or in conjunction with traditional imaging methods to better quantify regional tissue mechanics and/or establish biomechanical boundaries within tissues.

Conflict of interest disclosure

All authors were fully involved in the study and preparation of the manuscript and the manuscript is not being considered elsewhere for publication. All authors have no competing interests to disclose.

Acknowledgments

We thank Philip Buskohl for helpful discussions on the manuscript. This research was supported by the American Heart Association (#0830384N), the National Science Foundation (CBET-0955172) and the Cornell College of Engineering Learning Initiative Program.

References

Brommer, H., Laasanen, M.S., Brama, P.A., van Weeren, P.R., Helminen, H.J., Jurvelin, J.S., 2006. In situ and ex vivo evaluation of an arthroscopic indentation instrument to estimate the health status of articular cartilage in the equine metacarpophalangeal joint. Veterinary Surgery 35 (3), 259–266.

Buskohl, P.R., Gould, R.A., Butcher, J.T., 2012. Quantification of embryonic atrioventricular valve biomechanics during morphogenesis. Journal of Biomechanics 45 (5), 895–902.

Butcher, J.T., McQuinn, T.C., Sedmera, D., Turner, D., Markwald, R.R., 2007. Transitions in early embryonic atrioventricular valvular function correspond with

changes in cushion biomechanics that are predictable by tissue composition. Circulation Research 100 (10), 1503–1511.
Celi, S., Di Puccio, F., Forte, P., 2011. Advances in finite element simulations of elastosonography for breast lesion detection. Journal of Biomechanical Engineering 133 (8), 081006.
Cowin, S.C., Humphrey, J.D., 2002. Cardiovascular Soft Tissue Mechanics. Kluwer Academic Pub, Springer-Verlag, Inc., New York.
Chauveau, N., Hamzaoui, L., Rochaix, P., Rigaud, B., Voigt, J.J., Morucci, J.P., 1999. Ex vivo discrimination between normal and pathological tissues in human breast surgical biopsies using bioimpedance spectroscopy. Annals of the New York Academy of Sciences 873, 42–50.
Dawes-Higgs, E.K., Swain, M.V., Higgs, R.J., Appleyard, R.C., Kossard, S., 2004. Accuracy and reliability of a dynamic biomechanical skin measurement probe for the analysis of stiffness and viscoelasticity. Physiological Measurement 25 (1), 97–105.
Fung, Y.C., 1993. Biomechanics: Mechanical Properties of Living Tissues, Second ed. Springer-Verlag, New York.
Goyal, A., Newcombe, R.G., Chhabra, A., Mansel, R.E., 2008. Morbidity in breast cancer patients with sentinel node metastases undergoing delayed axillary lymph node dissection (ALND) compared with immediate ALND. Annals of Surgical Oncology 15 (1), 262–267.
Hendriks, F.M., Brokken, D., Oomens, C.W., Bader, D.L., Baaijens, F.P., 2006. The relative contributions of different skin layers to the mechanical behavior of human skin in vivo using suction experiments. Medical Engineering and Physics 28 (3), 259–266.
Hansma, P., Yu, H., Schultz, D., Rodriguez, A., Yurtsev, E.A., Orr, J., Tang, S., Miller, J., Wallace, J., Zok, F., Li, C., Souza, R., Proctor, A., Brimer, D., Nogues-Solan, X., Mellbovsky, L., Pena, M.J., Diez-Ferrer, O., Mathews, P., Randall, C., Kuo, A., Chen, C., Peters, M., Kohn, D., Buckley, J., Li, X., Pruitt, L., Diez-Perez, A., Alliston, T., Weaver, V., Lotz, J., 2009. The tissue diagnostic instrument. Review of Scientific Instruments 80 (5), 054303.
Ichikawa, T., Saito, K., Yoshioka, N., Tanimoto, A., Gokan, T., Takehara, Y., Kamura, T., Gabata, T., Murakami, T., Ito, K., Hirohashi, S., Nishie, A., Saito, Y., Onaya, H., Kuwatsuru, R., Morimoto, A., Ueda, K., Kurauchi, M., Breuer, J., 2010. Detection and characterization of focal liver lesions: a Japanese phase III, multicenter comparison between gadoxetic acid disodium-enhanced magnetic resonance imaging and contrast-enhanced computed tomography predominantly in patients with hepatocellular carcinoma and chronic liver disease. Investigative Radiology 45 (3), 133–141.
Jemec, G.B., Selvaag, E., Agren, M., Wulf, H.C., 2001. Measurement of the mechanical properties of skin with ballistometer and suction cup. Skin Research and Technology 7 (2), 122–126.
Jensen, M.O., Jensen, H., Honge, J.L., Hans, N., Hasenkam, J.M., Nielsen, S.L., 2012. External approach to in vivo force measurement on mitral valve traction suture. Journal of Biomechanics 45 (5), 908–912.
Kolb, T.M., Lichy, J., Newhouse, J.H., 2002. Comparison of the performance of screening mammography, physical examination, and breast US and evaluation of factors that influence them: an analysis of 27,825 patient evaluations. Radiology 225 (1), 165–175.
Kauer, M., Vuskovic, V., Dual, J., Szekely, G., Bajka, M., 2002. Inverse finite element characterization of soft tissues. Medical Image Analysis 6 (3), 275–287.
Karsdal M.A., Nielsen M.J., Sand J.M., Henriksen K., Genovese F., Bay-Jensen A.C., Victoria S., Adamkewicz J.I., Christiansen C., Leeming D.J., 2013. Extracellular matrix remodeling: the common denominator in connective tissue diseases possibilities for evaluation and current understanding of the matrix as more than a passive architecture, but a key player in tissue failure. Assay and Drug Development Technologies 11 (2), 70–92, http://dx.doi.org/10.1089/adt.2012.474.
Laughon, S.K., Zhang, J., Troendle, J., Sun, L., Reddy, U.M., 2011. Using a simplified Bishop score to predict vaginal delivery. Obstetrics and Gynecology 117 (4), 805–811.
Michaelson, J.S., Silverstein, M., Wyatt, J., Weber, G., Moore, R., Halpern, E., Kopans, D.B., Hughes, K., 2002. Predicting the survival of patients with breast carcinoma using tumor size. Cancer 95 (4), 713–723.
Nava, A., Mazza, E., Kleinermann, F., Avis, N.J., McClure, J., Bajka, M., 2004. Evaluation of the mechanical properties of human liver and kidney through aspiration experiments. Technology and Health Care 12 (3), 269–280.
Oberai, A.A., Gokhale, N.H., Goenezen, S., Barbone, P.E., Hall, T.J., Sommer, A.M., Jiang, J., 2009. Linear and nonlinear elasticity imaging of soft tissue in vivo: demonstration of feasibility. Physics in Medicine and Biology 54 (5), 1191–1207.
Robben, J.H., Pollak, Y.W., Kirpensteijn, J., Boroffka, S.A., van den Ingh, T.S., Teske, E., Voorhout, G., 2005. Comparison of ultrasonography, computed tomography, and single-photon emission computed tomography for the detection and localization of canine insulinoma. Journal of Veterinary Internal Medicine 19 (1), 15–22.
Samani, A., Plewes, D., 2007. An inverse problem solution for measuring the elastic modulus of intact ex vivo breast tissue tumours. Physics in Medicine and Biology 52 (5), 1247–1260.
Shen C., Ramkumar A., Lal A., Gilmour R.F., 2010. Wireless transmission of cardiac action potentials with ultrasonically guided insertion of silicon probes. In: Conference Proceedings of IEEE Engineering in Medicine and Biology Society, pp. 5022–5025.
Vasara, A.I., Jurvelin, J.S., Peterson, L., Kiviranta, I., 2005. Arthroscopic cartilage indentation and cartilage lesions of anterior cruciate ligament-deficient knees. American Journal of Sports Medicine 33 (3), 408–414.
Yan, C., Cho, J.H., Ahn, J.H., 2012. Graphene-based flexible and stretchable thin film transistors. Nanoscale 4 (16), 4870–4882.